

Flexing the Muscles of *m*-Divinylbenzene: Direct Measurement of the Barriers to Conformational Isomerization[†]

Talitha M. Selby[‡] and Timothy S. Zwier*[‡]

Department of Chemistry, Purdue University, West Lafayette, Indiana 47907-2084

Received: December 1, 2006; In Final Form: January 22, 2007

The energy thresholds to isomerization of the three conformational isomers of *m*-divinylbenzene (*cis*–*cis*, *cis*–*trans*, and *trans*–*trans*) were directly measured by stimulated emission pumping–population transfer (SEP–PT) spectroscopy. The experimentally determined isomerization thresholds are $E_{\text{thresh}}(cc \rightarrow ct, tt) = 1080\text{--}1232\text{ cm}^{-1}$, $E_{\text{thresh}}(tt \rightarrow ct, cc) = 1130\text{--}1175\text{ cm}^{-1}$, $E_{\text{thresh}}(ct \rightarrow cc) = 997\text{--}1175\text{ cm}^{-1}$, and $E_{\text{thresh}}(ct \rightarrow tt) = 997\text{--}1232\text{ cm}^{-1}$. On the basis of the threshold values for $X \rightarrow Y$ and $Y \rightarrow X$ isomerization, the relative energies of the conformational isomers are $-102 \leq E(ct) \leq +178\text{ cm}^{-1}$ and $-102 \leq E(cc) \leq +95\text{ cm}^{-1}$ relative to $E(tt) = 0$. UV-hole-filling (UVHF) spectroscopy was also used to determine the effect of population returning to the ground state via fluorescence. A full set of governing equations for SEP–PT and UVHF spectroscopy is reported that will be generally useful for future studies using these methods. By comparison of these results with the computed stationary points on a calculated surface (DFT B3LYP/6-31+G*), the isomerization pathway was determined to involve sequential isomerization of each vinyl group rather than concerted motion. The energy thresholds were also combined with the ground state torsional vibrational energy levels to obtain a new fitted two-dimensional torsional potential for *m*DVB.

I. Introduction

In the preceding paper¹ the ultraviolet spectroscopy of the three conformers of *m*-divinylbenzene (*m*DVB) (Figure 1) was explored. The low-frequency regions of the S_0 – S_1 spectra exhibited vibronic structure due to the torsional degrees of freedom of the two vinyl groups, presenting a model system in which to explore the degree to which this structure could be used to determine the barrier heights and shape of the two-dimensional torsional potential energy surface. The computed relaxed torsional potential energy surface (DFT B3LYP/6-31+G*) is reproduced here (Figure 1) for easy reference in what follows. The barriers to isomerization of a single vinyl group extracted from this fitting procedure showed a strong correlation between the key fitting parameters, especially V_2 , V_{22}^c , and V_4 , leading to a range of parameters with barrier heights for isomerization that varied from 500 to 1400 cm^{-1} . Furthermore, the relative energies of the minima were not determined with any accuracy by the experimental torsional level data, which did not reach up into the energy region near the tops of the barriers where the relative energies of the wells would begin to play a role. Thus, it was clear from this fitting that aspects of the two-dimensional torsional potential were difficult to pin down with any accuracy from the low-lying torsional levels alone.

On the basis of the results and analysis in the preceding paper,¹ there is a clear need for an alternative measurement of the energy barriers to isomerization. We therefore decided to carry out a second study to determine the lowest-energy isomerization thresholds between all six reactant–product pairs

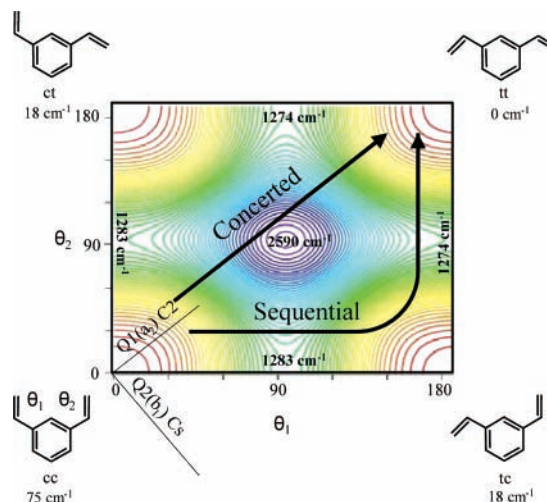


Figure 1. Relaxed potential energy surface calculated at the DFT/B3LYP//6-31+G* level of theory at a 4° step size. The relative energies of the minima and transition states are the ZPE-corrected values.

of *m*DVB by direct measurement using stimulated emission pumping–population transfer spectroscopy (SEP–PT).^{2–7} The method shares some features in common with the SEP–R2PI methods used by Leutwyler and co-workers to measure the binding energies of complexes.^{8,9} In the present context, SEP is used to initiate conformational isomerization in a single conformational isomer beginning with a well-defined but tunable internal energy. As we shall see, the method asks and answers a simple “yes/no” question regarding the isomerization, signaling with the first appearance of population in the product that the threshold to isomerization to form that product has been overcome. In this sense, the method is completely complementary to the torsional level spectroscopy in that it is sensitive only to the barrier heights but tells us little about the shape of

[†] Part of the special issue “James A. Miller Festschrift”.

* Corresponding author. E-mail: zwier@purdue.edu. Phone: (765) 494-5278. Fax: (765) 494-5330.

[‡] Present address: Sandia National Laboratories, Combustion Research Facility, Mail Stop 9055, Livermore, CA 94551.

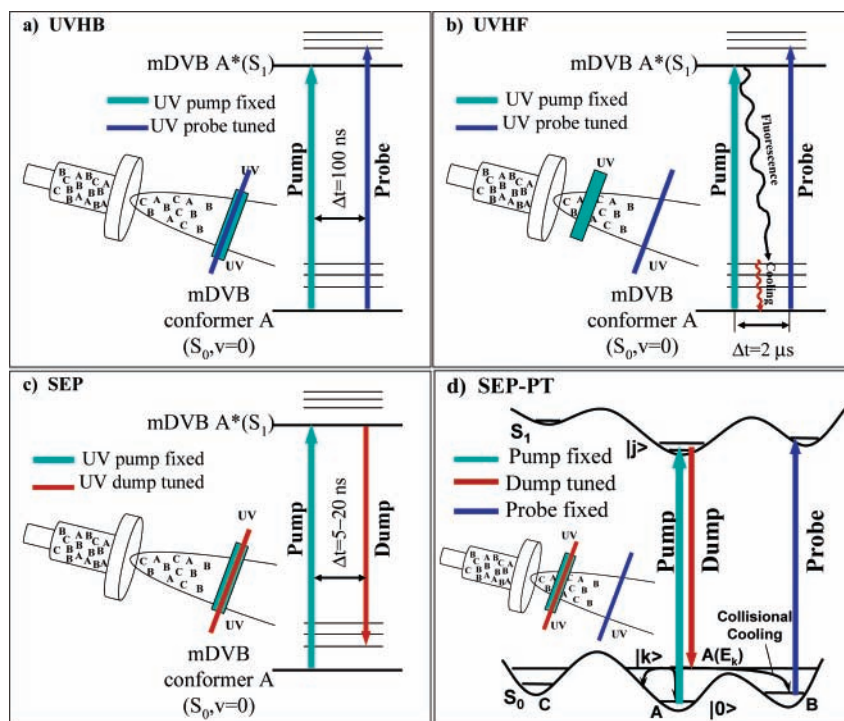


Figure 2. Energy level, spatial, and timing diagrams for (a) UVHB, (b) UVHF, (c) SEP, and (d) SEP–PT spectroscopy.

the torsional potential energy surface in the regions near the minima (as the vibronic spectroscopy can). Because the vinyl “appendages” and phenyl “body” of *m*DVB bear some resemblance to a human’s upper torso (Figure 1), we refer to the laser-initiated conformational isomerization as “flexing the muscles” of *m*DVB.

The present study also addresses the pathway for isomerization. The measured threshold for *cc* ↔ *tt* isomerization will indicate whether the preferred pathway is sequential (occurring by flexing one vinyl appendage at a time) or concerted (flexing both simultaneously). In the former case, the isomerization pathway would involve motion along one torsional coordinate and then the other, skirting around the periphery of the torsional surface (Figure 1). In doing so, the nuclear motion would involve traversing two barriers in the 1000–1300 cm^{-1} range in which first one vinyl group is rotated perpendicular to the phenyl ring and then the other. In the case of a concerted pathway, motion would occur along the diagonal or antidiagonal to saddle points of approximately twice the height.

II. Experimental Methods and Intensity Equations

The primary spectroscopic tool used in the present study is the triple resonance method of stimulated emission pumping–population transfer (SEP–PT) spectroscopy.^{2–7} However, the method has a close and obvious connection with other double-resonance methods that employ two of the three lasers used in the SEP–PT experiment. A quantitative understanding of the intensities in the SEP–PT spectrum therefore benefits from consideration of the two-laser experiments on which it is built. In this section, we introduce the double resonance methods of UV holeburning (UVHB),¹⁰ UV hole-filling (UVHF), and stimulated emission pumping (SEP)¹¹ and develop intensity expressions for SEP–PT that involve these contributions. We develop these equations here because they provide a deeper understanding of the observed changes in intensity with internal energy observed in the SEP–PT scans. To assist the discussion, an energy level and spatial diagram that summarizes the methods is shown in Figure 2.

All experiments were carried out in the same LIF chamber used in the preceding paper.¹ The supersonic free jet was produced by pulsed expansion (general valve, series 9) through a 1.2 mm diameter nozzle orifice. *m*DVB was entrained in the expansion by flowing helium (7 bar) over a reservoir of the liquid held at room temperature. The doubled outputs of three Nd:YAG-pumped dye lasers operating in the 310–335 nm region were used as the excitation sources, each with ~8 ns pulse duration. All the methods measure the fractional population change in the signal due to one laser induced by another laser or lasers. This was accomplished either using the active baseline subtraction mode of the gated integrator or via a LabView program that recorded the difference in software.

II.1. UVHB Spectroscopy. UVHB spectroscopy was described in the preceding article, where resonant two-photon ionization was used in the detection step.¹ In the present work, UVHB spectra were recorded under similar conditions to the hole-filling experiments for comparison with them, using laser-induced fluorescence (LIF) in the probe step. For this purpose, the doubled output of a Nd:YAG-pumped, tunable dye laser (hereafter called the “pump” laser) operating at 10 Hz was fixed on the $0 \rightarrow j$ vibronic transition of a particular isomer, intersecting the supersonic free jet 10 nozzle diameters downstream from the nozzle orifice (i.e., $x/D \approx 10$, $D = 1.2$ mm diameter). The power of this pump laser (~0.3 mJ/pulse at 10 Hz) was sufficient to partially saturate the transition on which it is fixed, thereby burning a “hole” in the ground state population. A second probe laser (~0.05 mJ/pulse at 20 Hz) interrogated the same molecules $2 \mu\text{s}$ later at $x/D \approx 14$. UVHB spectra were recorded by tuning the probe laser through the $S_1 \leftarrow S_0$ vibronic transitions of interest. When the probe laser was resonant with a transition that shared the same ground state level as the transition on which the pump laser was fixed, the ground state population was partially depleted by the pump laser, leading to a smaller probe laser signal. The difference between the LIF signal with and without the pump laser present was monitored. When normalized to the total LIF signal of the probe laser at that frequency, the intensity of a transition in the UVHB

spectrum, $I_A^{\text{UVHB}}(\tilde{\nu}_{0j})$, measures the fractional depletion in population of the zero-point level of conformer A caused by the pump laser:

$$I_A^{\text{HB}}(\tilde{\nu}_{0j}, \tilde{\nu}_{\text{probe}}) = \frac{\Delta N_A^{\text{HB}}(\tilde{\nu}_{\text{probe}})}{N_A} \quad (1)$$

Since $\Delta N_A^{\text{HB}} < 0$, I_A^{HB} is a negative quantity. A gating circuit was used to turn on the photomultiplier tube (PMT) after the pump laser fired to prevent saturation of the PMT.

II.2. SEP Spectroscopy. Stimulated emission pumping (SEP) spectra of each conformer (Figure 2c) were recorded by fixing the wavelength of a UV laser (pump laser, ~ 0.05 – 0.2 mJ/pulse, 20 Hz) on the $0 \rightarrow j$ vibronic transition of a particular conformer (e.g., conformer A) and tuning a second high powered UV laser (dump laser, ~ 0.4 – 1.0 mJ/pulse, 10 Hz) over a wavelength range where transitions from $|j\rangle$ back down to vibrational levels $|k\rangle$ in the ground state could be interrogated. The timing delay between the pump and dump lasers was kept short (5–20 ns) relative to the excited state lifetime of the molecule ($\tau(S_1 \text{ origin}) \sim 80$ ns). When the dump laser frequency $\tilde{\nu}_{jk}$ was resonant with an SEP transition from $|j\rangle$ to $|k\rangle$, the dump laser partially depleted the excited state population, causing a decrease in the total fluorescence decay signal. This depletion was monitored with a gated integrator in active baseline subtraction, with the gate fixed on the trailing edge of the fluorescence decay curve. When normalized to the total fluorescence signal, the intensity of a transition in the SEP spectrum, $I_A^{\text{SEP}}(\tilde{\nu}_{jk})$, measures the fraction of the excited state population in $|j\rangle$ that is transferred by the dump laser to ground state level $|k\rangle$ and is a negative quantity.

II.3. UVHF Spectroscopy. UV hole-filling spectroscopy (UVHF) employs a similar configuration to UVHB, except that the nozzle position was moved relative to the pump and probe lasers (Figure 2b) into “hole-filling” conditions. These conditions comprise a “cool–excite–cool–probe” experimental protocol that has been used in a number of previous studies.^{2–7,12–14} Initial cooling of the conformer population occurred prior to pump laser excitation at $x/D \sim 2$. In UVHF, the pump laser was fixed on the $0 \rightarrow j$ vibronic transition of one conformer, as in UVHB. Following excitation, a fraction of the population can return to the ground state via fluorescence or nonradiative processes. Under many circumstances, the fluorescence quantum yield is small, and the molecules returning to the ground state via nonradiative processes cannot be cooled sufficiently to be returned to the zero-point level probed by the probe laser. Then the UVHF intensities will equal those in UVHB.

On the other hand, if the fluorescence quantum yield is large and/or the collisional cooling of highly internally excited molecules created by nonradiative pathways is efficient, then a fraction of the excited population could be cooled back into the reactant zero-point level (f_{AA}^{recool}) or, after isomerization, be cooled into the zero-point level of product conformer B (f_{AB}^{recool}). In the former case, this returning population partially fills in the population hole created by the pump laser, accounting for the method’s name. The probe laser is then tuned through the transitions of interest while the difference in probe signal induced by the pump laser was recorded, as in UVHB.

The intensity of a transition in the UVHF spectrum depends on whether the reactant “A” (eq 2a) or the product “B” (eq 2b) is monitored with the probe laser:

$$I_{AA}^{\text{UVHF}}(\tilde{\nu}_{\text{probe}}) = I_A^{\text{HB,up}}(\tilde{\nu}_{0j}) [1 - f_{AA}^{\text{recool}}] \quad (2a)$$

$$I_{AB}^{\text{UVHF}}(\tilde{\nu}_{\text{probe}}) = -I_A^{\text{HB,up}}(\tilde{\nu}_{0j}) \left(\frac{F_A}{F_B} \right) f_{AB}^{\text{recool}} \quad (2b)$$

After normalization to the probe signal in the absence of the pump laser, the intensity of a UVHF transition can be equated with the fractional change in population of reactant “A” or product “B” caused by the pump laser under hole-filling conditions. The minus sign in front of eq 2b is needed because the UVHF signal in the product channel is a gain signal while UVHB intensity is negative. In these equations, we have explicitly included a reminder that the UVHB intensity, $I_A^{\text{HB,up}}(\tilde{\nu}_{0j})$, must be recorded under the “upstream” conditions appropriate for the UVHF spectrum. F_A and F_B are the fractional populations of the reactant and product conformers in the absence of any laser excitation. The ratio (F_A/F_B) then corrects for the fact that the UVHF signal is a fractional change in the population of conformer B, recognizing that this fractional change will depend on whether the excited conformer A has a large or small fractional abundance to begin with.

II.4. SEP–PT Spectroscopy. Stimulated emission pumping–population transfer spectroscopy (SEP–PT, Figure 2d)^{2–7} was used to determine the energy thresholds for isomerization of the six reactant–product pairs of mDVB ($cc \leftrightarrow tt$, $ct \leftrightarrow tt$, and $cc \leftrightarrow ct$). SEP–PT employs hole-filling conditions (Figure 2d), with pump and dump lasers spatially overlapped at $x/D \sim 2$, and $\Delta t_{12} = 5$ – 20 ns. As in SEP, the pump laser was fixed on the $S_1 \leftarrow S_0$ origin transition of the reactant conformer (e.g., conformer A) and the dump laser was tuned through the SEP spectrum. In SEP–PT, the probe laser beam was spatially separated from pump and dump by 5–7 mm and delayed by $\Delta t_{23} \sim 2 \mu\text{s}$, a time sufficient for SEP excited molecules to traverse the distance between the laser beams. The probe laser had its wavelength fixed on an $S_1 \leftarrow S_0$ origin transition of the conformer of choice (e.g., conformer B).

The difference signal recorded by SEP–PT spectroscopy is the difference in probe laser signal between that with both pump and dump lasers present and that with pump alone:

$$\Delta I_{\text{probe}}(\text{SEP–PT}) = I_{\text{probe}}(\text{pump} + \text{dump}) - I_{\text{probe}}(\text{pump only}) \quad (3)$$

This is accomplished by pulsing the pump and probe lasers at 20 Hz and the dump laser at 10 Hz so that the dump laser is only present every other probe laser pulse. When the pump laser alone is present, the probe signal is modified by the action of the pump laser on the probed conformer population. This is equivalent to the “pump on” signal in a UVHF spectrum.

When both the pump and dump lasers are present, the dump laser transfers a fraction of the excited population back to a particular ground state energy level E_k , and it is this population that we seek to detect following its isomerization and recooling. At the same time, the dump laser also decreases the excited state population, thereby decreasing the fractional population that returns to the ground state from A^* by f_{AA}^{SEP} for reactant A and by $(F_A/F_B)I_A^{\text{SEP}} f_{AB}^{\text{recool}}$ for product B.

On the basis of these considerations, intensity equations for SEP–PT have been developed that explicitly include the competition between the SEP and “pump only” pathways for returning to the ground state. As previously, we consider a series of SEP–PT spectra in which (i) the 20 Hz pump laser is fixed on transition $0 \rightarrow j$ of conformer A (the “reactant”), (ii) the 10 Hz SEP dump laser is tuned through a series of $j \rightarrow k$ transitions back to the ground state of A with energies E_k , and (iii) the 20 Hz probe laser is fixed on the $S_1 \leftarrow S_0$ origin transition of a

reactant (A) or product (B) conformer. The equations governing the intensity of the $j \rightarrow k$ “dump” transition in the SEP–PT spectra when monitoring reactant A (eq 2a) or product B (eqs 2b and 2c) are given by

$$I_{AA}^{\text{SEP-PT}}(\tilde{\nu}_{jk}) = I_A^{\text{HB,up}}(\tilde{\nu}_{0j}) \cdot I_A^{\text{SEP,up}}(\tilde{\nu}_{jk}) [\Phi_{AA}(E_k) - f_{AA}^{\text{recool}}] \quad (4a)$$

$$I_{AB}^{\text{SEP-PT}}(\tilde{\nu}_{jk}) = \left(\frac{F_A}{F_B}\right) I_A^{\text{HB,up}}(\tilde{\nu}_{0j}) \cdot I_A^{\text{SEP,up}}(\tilde{\nu}_{jk}) [\Phi_{AB}(E_k) - f_{AB}^{\text{recool}}] \quad (4b)$$

where most of the quantities have been previously defined. In these equations, we assume that the pump and probe lasers move the population independently and sequentially, an assumption that is met in the present case because the delay between pump and dump lasers (5–20 ns) is comparable to or greater than the pump pulse duration (~8 ns). The product $I_A^{\text{HB,up}}(\tilde{\nu}_{0j}) \cdot I_A^{\text{SEP,up}}(\tilde{\nu}_{jk})$ can be interpreted as the fractional population transferred from the zero-point level of “A” to level E_k by the joint action of pump and dump lasers. $\Phi_{AX}(E_k)$ is the isomerization quantum yield for formation of X starting from level E_k in conformer A. The competition between SEP-induced population change and population change initiated by the pump laser alone is evident in the difference of the two terms in square brackets.

For SEP transitions to levels with energy E_k less than the lowest isomerization threshold, all population brought to the ground state via the dump transition will remain in the reactant well “A” and be recooled to the zero-point level of A; that is, $\Phi_{AA}(E_k) = 1$ and $\Phi_{AX}(E_k) = 0$ when $X \neq A$. Equations 4a and 4b then become

$$I_{AA}^{\text{SEP-PT}}(\tilde{\nu}_{jk}) = I_A^{\text{HB,up}}(\tilde{\nu}_{0j}) \cdot I_A^{\text{SEP,up}}(\tilde{\nu}_{jk}) (1 - f_{AA}^{\text{recool}}) \quad \text{for} \\ E_k < E_{\text{lowest threshold}} \quad (5a)$$

and

$$I_{AB}^{\text{SEP-PT}}(\tilde{\nu}_{jk}) = \left(\frac{F_A}{F_B}\right) I_A^{\text{HB,up}}(\tilde{\nu}_{0j}) \cdot I_A^{\text{SEP,up}}(\tilde{\nu}_{jk}) (-f_{AB}^{\text{recool}}) \quad \text{for} \\ E_k < E_{\text{lowest threshold}} \quad (5b)$$

As a result, dump transitions to levels below the lowest energy threshold will show a *depletion* in the product channels if f_{AB}^{recool} is sufficiently large to be measurable.

Comparing eqs 4 and 2, we see that eq 4 can be recast in terms of UVHF intensities:

$$I_{AA}^{\text{SEP-PT}}(\tilde{\nu}_{jk}) = I_A^{\text{SEP,up}}(\tilde{\nu}_{jk}) \cdot [I_{AA}^{\text{UVHF}}(\tilde{\nu}_{\text{probe}}) + I_A^{\text{HB,up}}(\tilde{\nu}_{0j}) (\Phi_{AA}(E_k) - 1)] \quad (6a)$$

$$I_{AB}^{\text{SEP-PT}}(\tilde{\nu}_{jk}) = I_A^{\text{SEP,up}}(\tilde{\nu}_{jk}) \cdot \left[I_{AB}^{\text{UVHF}}(\tilde{\nu}_{\text{probe}}) + \left(\frac{F_A}{F_B}\right) I_A^{\text{HB,up}}(\tilde{\nu}_{0j}) \Phi_{AB}(E_k) \right] \quad (6b)$$

This form of the equations is useful in that it involves quantities that, at least in principle, can be measured experimentally, including the fractional abundances (from IR–PT studies),¹ SEP, UVHF, and UVHB intensities. The latter quantities must be measured under identical conditions to the SEP–PT measurement, which is made difficult by interference from scattered light when the laser beams cross the expansion near the exit

face of the pulsed valve. Equations 6a and 6b are quite general in that they hold no matter what the size or source of the pump laser-induced, recooled population.

In its most general form, f_{AX}^{recool} is a sum of three terms (eq 7) due to fluorescence, internal conversion, and intersystem crossing:

$$f_{AX}^{\text{recool}} = \phi_f^A \Phi_{AX}^f \phi_{\text{coll},f} + \phi_{\text{IC}}^A \Phi_{AX}^{\text{IC}} \phi_{\text{coll,IC}} + \phi_{\text{ISC}}^A \Phi_{AX}^{\text{ISC}} \phi_{\text{coll,ISC}} \quad (7)$$

Thus, the population that is not removed by the SEP dump transition divides into three subpopulations: one that is trapped in the triplet state (on the time scale of the experiment), one in which the full 32 000 cm^{-1} of UV excitation energy resides in high-lying vibrational levels in the ground state due to internal conversion, and a ground state population with 0–3000 cm^{-1} vibrational energy following fluorescence to the Franck–Condon active ground state levels. In eq 7, ϕ_f^A is the fluorescence quantum yield for conformer A, Φ_{AX}^f is the product quantum yield for formation of X from A from the ground state population created by fluorescence, and the IC and ISC labels denote the corresponding quantities due to internal conversion and intersystem crossing, respectively. ϕ_{coll} is the collection efficiency for recoiling to the zero-point level the subpopulations arriving at the ground state via fluorescence, internal conversion, or intersystem crossing.

By proper choice of cooling conditions (e.g., by varying the separation between the pump and probe lasers or the collision frequency at the point of pump excitation), it should be possible to recool to the zero-point level the molecules reaching the ground state via fluorescence ($\phi_{\text{coll},f} = 1$), but leave the other molecules undergoing internal conversion or intersystem crossing with sufficient internal energy (either electronic or vibrational) that their contribution to the probe laser signal is negligible, as in UVHB ($\phi_{\text{coll,ISC}} = \phi_{\text{coll,IC}} = 0$). In this case, $f_{AX}^{\text{recool}} = \phi_f^A \Phi_{AX}^f$, and the SEP–PT intensity equations become

$$I_{AA}^{\text{SEP-PT}}(\tilde{\nu}_{jk}) = I_A^{\text{HB,up}}(\tilde{\nu}_{0j}) \cdot I_A^{\text{SEP,up}}(\tilde{\nu}_{jk}) [\varphi_{AA}(E_k) - (\phi_f^A \Phi_{AA}^f)] \quad (8a)$$

$$I_{AB}^{\text{SEP-PT}}(\tilde{\nu}_{jk}) = \left(\frac{F_A}{F_B}\right) I_A^{\text{HB,up}}(\tilde{\nu}_{0j}) \cdot I_A^{\text{SEP,up}}(\tilde{\nu}_{jk}) [\Phi_{AB}(E_k) - (\phi_f^A \Phi_{AB}^f)] \quad (8b)$$

If, in addition, the fluorescence quantum yield ϕ_f^A is sufficiently small, $f_{AX}^{\text{recool}} \approx 0$, and the SEP–PT intensity equations reduce to

$$I_{AA}^{\text{SEP-PT}}(\tilde{\nu}_{jk}) = I_A^{\text{HB,up}}(\tilde{\nu}_{0j}) \cdot I_A^{\text{SEP,up}}(\tilde{\nu}_{jk}) \Phi_{AA}(E_k) \quad (9a)$$

$$I_{AB}^{\text{SEP-PT}}(\tilde{\nu}_{jk}) = \left(\frac{F_A}{F_B}\right) I_A^{\text{HB,up}}(\tilde{\nu}_{0j}) \cdot I_A^{\text{SEP,up}}(\tilde{\nu}_{jk}) \Phi_{AB}(E_k) \quad (9b)$$

In the limit that eqs 9a and 9b hold, the energy threshold for $A \rightarrow B$ conformational isomerization can be easily identified. Below the $A \rightarrow B$ energy threshold E_{thresh} , $\Phi_{AB}(E_k < E_{\text{thresh}}) = 0$, and therefore $I_{AB}^{\text{SEP-PT}}(\tilde{\nu}_{jk}) = 0$; that is, there is no SEP–PT signal in the product channel. By contrast, once $E_k > E_{\text{thresh}}$, $\Phi_{AB}(E_k > E_{\text{thresh}}) > 0$, and $I_{AB}^{\text{SEP-PT}}(\tilde{\nu}_{jk})$ exhibits a gain signal whose magnitude depends on the magnitude of $\Phi_{AB}(E_k)$ and the amount of population transferred to level E_k via the pump–dump combination. This is the “yes/no” answer that is a particular strength of the method in measuring barrier heights.

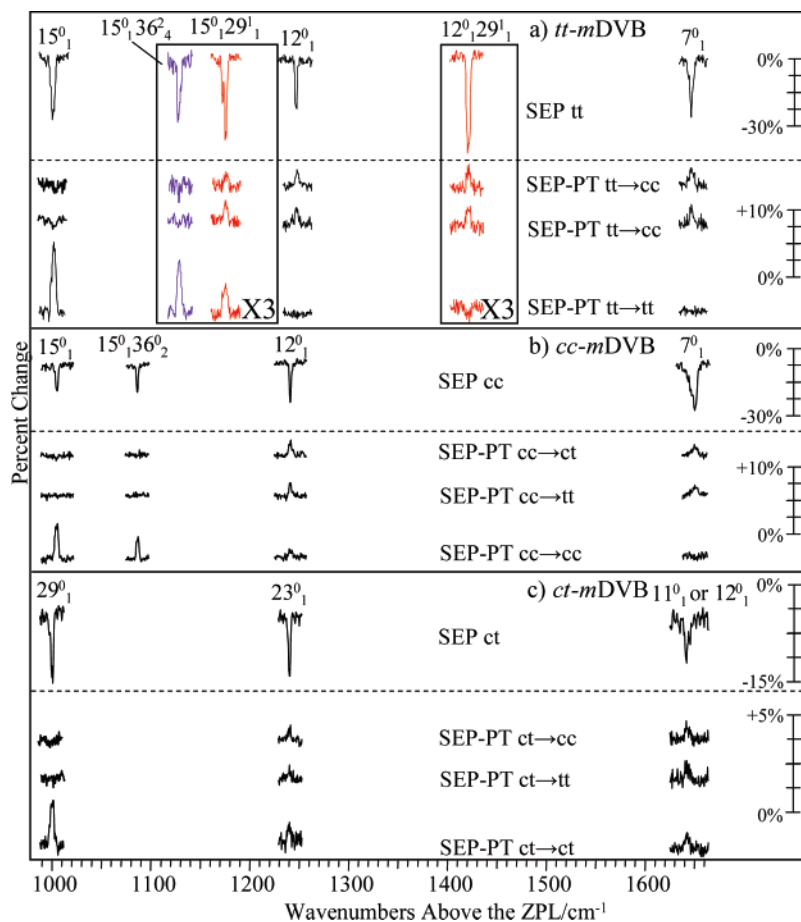


Figure 3. SEP and SEP-PT spectra of (a) *tt*-*mDVB*, (b) *cc*-*mDVB*, and (c) *ct*-*mDVB*. The top traces are SEP spectra, the middle two traces are SEP-PT spectra into products, and the bottom traces are SEP-PT spectra monitoring the initially excited “reactant”. The black traces indicate SEP transitions from the S_1 origin, and the purple and red traces indicate SEP transitions in *tt*-*mDVB* out of the 36^2 and 29^1 S_1 vibronic levels, 127 and 174 cm^{-1} above the S_1 origin transition, respectively.

In this limit, the first observed dump transition in the product X channel constitutes an upper bound to the $A \rightarrow X$ energy threshold, while the last unobserved SEP transition that is strong enough to have been observed serves as a lower bound.

The energy threshold is also reflected in a corresponding change in the gain signal in the reactant channel. Below the lowest $A \rightarrow$ product threshold, $\Phi_{AA}(E_k < E_{\text{thresh}}) = 1$ and

$$I_{AA}^{\text{SEP-PT}}(\tilde{\nu}_{jk}) = I_A^{\text{HB,up}}(\tilde{\nu}_{0j}) I_A^{\text{SEP,up}}(\tilde{\nu}_{jk}) \quad (10)$$

Thus, below the lowest threshold, the reactant channel will show a large gain signal equal in magnitude to the total fractional population of A driven to energy level E_k by the pump and dump lasers. Once the lowest energy threshold has been overcome, $\Phi_{AA}(E_k > E_{\text{thresh}}(B))$ is reduced to $\Phi_{AA} = 1 - \Phi_{AB}$ and then is reduced still further as the barriers to other conformational products are overcome.

III. Results and Analysis

1. SEP and SEP-PT Spectra. The SEP and SEP-PT spectra for the conformers of *mDVB* are shown in Figure 3. In all the scans, the abscissa is the difference in photon energy between the pump and dump lasers, plotted here as the internal energy residing in the excited conformer after the dump transition. A total of 12 spectra is shown, 4 for each of the 3 conformational reactants *tt* (Figure 3a), *cc* (Figure 3b), and *ct* (Figure 3c). In each set of four, the top traces show the SEP spectra of the respective reactants recorded with pump laser

fixed on the $S_1 \leftarrow S_0$ origin (black traces). The scale on the right above the dotted line in each section of Figure 3 is a percent depletion in the indicated conformer’s excited state population induced by the dump laser. The two middle traces show the SEP-PT spectra from the indicated reactant into each of the two possible products. Finally, the bottom traces show the SEP-PT spectra monitoring the reactant channel (e.g., *tt* \rightarrow *tt*). The corresponding scale below the dotted lines denotes the percent gain in the indicated product population. The SEP-PT spectra were obtained by tuning locally over regions of strong SEP transitions in the anticipated region of the isomerization barrier. This tactic was chosen, rather than continuous scans over the entire region, due to the small amount of population transferred in these studies. The expanded scale for the *ct* conformer indicates that it was not possible to move as much population via the pump and dump lasers in the *ct* conformer as in the others. This is a result of the lower oscillator strength noted in the preceding paper¹ for this conformer.

In all three SEP spectra from the S_1 origins (Figure 3a–c top traces) the strongest SEP transitions occur at ~ 1000 , 1250 , and 1650 cm^{-1} (shown in black). The specific vibronic transitions responsible for each band are given in the figure, using the vibrational numbering schemes introduced in the preceding paper for each *mDVB* conformer.¹ In *cc*-*mDVB*, an additional transition can be observed in the SEP spectrum at 1080 cm^{-1} (assigned to $150^0_136^0_2$).

In an attempt to find additional SEP dump transitions that produce reactants with internal energies between the main bands

present in the S_1 origin SEP spectra, the dispersed fluorescence spectra from the preceding paper¹ were used to identify upper vibronic levels with strong emission into bands in the gap between the lower and upper bounds from the origin SEP spectra. On that basis, in *tt*-*m*DVB, SEP spectra were taken using pump transitions 127 and 174 cm^{-1} above the S_1 origin, assigned to the overtone of the out-of-plane vinyl torsion (36_0^2) and the fundamental of the in-plane vinyl bend (29_0^1), respectively. The former possessed one SEP transition at 1130 cm^{-1} (in purple) and the latter two additional SEP transitions (with internal energies of 1175 and 1421 cm^{-1} , in red) that were found to have sufficient intensity to be useful. Unfortunately, analogous transitions with sufficient intensity to drive measurable population in the SEP–PT experiment were not found for the *cc* and *ct* isomers. In particular, higher-lying vibronic bands in the excitation spectrum, which were viewed as potential candidates (via their DFL spectra), could not be used to generate strong SEP signals. It seems likely that these intermediate levels experienced intramolecular vibrational redistribution (IVR) or collisional relaxation that dilutes the intensity of the emitting transitions back down to the ground state in such a way that strong SEP signals were not possible.

We check first the intensity of SEP–PT traces to product channels (middle traces in Figure 3) at low energies anticipated to be below the lowest barrier to isomerization. The SEP transitions near 1000 cm^{-1} in all three conformers show no measurable depletion, consistent with $f_{\text{AX}}^{\text{recool}} \approx 0$ in eq 5b. As a result, we can use SEP–PT intensity expressions for the product channels that hold in this limit (eqs 9 and 10) and interpret the onset of measurable gain in population in a given product channel as an unequivocal indicator that the barrier to isomerization has been overcome. At the same time, in the reactant channel, a maximum population gain is observed for the 1000 cm^{-1} SEP–PT transitions, consistent with all the “dumped” population being funneled back entirely to the reactant zero-point level.

In *tt*-*m*DVB (Figure 3a), the SEP–PT spectra with dump transition at 1130 cm^{-1} ($15_0^1 36_4^2$) produced no population gain in either *ct* or *cc* product channels. However, at 1175 cm^{-1} ($15_0^1 29_1^1$), clear gain is observed in both populations. Thus, the thresholds to both *tt* \rightarrow *cc* and *tt* \rightarrow *ct* isomerization are between 1130 and 1175 cm^{-1} . In *ct*-*m*DVB (Figure 3c), the only strong SEP transitions in the barrier region are at 997 and 1243 cm^{-1} . Therefore, the thresholds to *ct* \rightarrow *tt* and *ct* \rightarrow *cc* isomerization can only be bracketed between 997 and 1243 cm^{-1} . In *cc*-*m*DVB (Figure 3b), the additional strong SEP transition at 1080 cm^{-1} internal energy shows no product gains but a clear gain in the reactant. Hence, the thresholds to *cc* \rightarrow *tt* and *cc* \rightarrow *ct* isomerization are both between 1080 and 1232 cm^{-1} .

The SEP–PT intensity (eq 9) can also be used to estimate the relative product quantum yields for SEP–PT transitions above the barriers to isomerization. Given the small SEP–PT signal sizes and other sources of error, we choose to use the data only to draw general conclusions and to illustrate the method of extracting quantum yields from the data. From eq 9b, one can see that the ratio of SEP–PT intensities of a given transition in the two *m*DVB product channels is given by

$$\frac{I_{\text{AB}}^{\text{SEP-PT}}(\tilde{\nu}_{jk})}{I_{\text{AC}}^{\text{SEP-PT}}(\tilde{\nu}_{jk})} = \left(\frac{F_{\text{C}}}{F_{\text{B}}} \right) \frac{\Phi_{\text{AB}}(E_k)}{\Phi_{\text{AC}}(E_k)} \quad (11)$$

Independent of which conformer is initially excited (*tt*, *cc*, or *ct*) and the internal energy above the barrier (1240, 1422, or

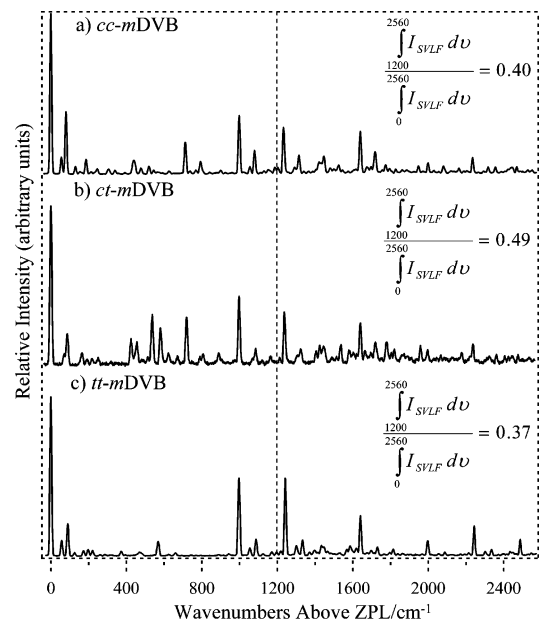


Figure 4. Dispersed fluorescence spectra of the $S_1 \leftarrow S_0$ origin transitions of (a) *cc*-*m*DVB, (b) *ct*-*m*DVB, and (c) *tt*-*m*DVB. The dotted line at 1200 cm^{-1} denotes the determined energy thresholds for isomerization. The percent fluorescence, which is above the isomerization threshold for each isomer, is indicated.

1640 cm^{-1}), the intensities of the SEP–PT gains in the two product channels are always nearly equal in size, so that their ratio is approximately 1.0. In *m*DVB, the fractional abundances have been determined from IR–PTS studies¹ to be $F_{cc} = 0.31 \pm 0.08$, $F_{ct} = 0.39 \pm 0.15$, and $F_{tt} = 0.30 \pm 0.07$. Thus, to a first approximation, these fractional abundances can also be considered equal. This indicates that in every case, the population is being distributed roughly equally between the two products; that is, $\Phi_{\text{AB}}(E_k) \sim \Phi_{\text{AC}}(E_k)$.

One puzzling aspect of this deduction is that it suggests, based on eq 9a, that the reactant channels should show a similar sized gain to those in the products. However, SEP–PT scans over the 1240 and 1640 cm^{-1} *tt* \rightarrow *tt* and *cc* \rightarrow *cc* reactant channels show no measurable gain signal. On this basis, one is led to surmise that $\Phi_{\text{AA}} \sim 0$, an answer that makes little physical sense. The likely source of error here is in assuming that if $f_{\text{AB}}^{\text{recool}}$ is negligible, then $f_{\text{AA}}^{\text{recool}}$ will also be negligible. If the major contribution to the recooled population is from fluorescence, then $f_{\text{AA}}^{\text{recool}} = \phi_{\text{f}}^{\text{A}} \Phi_{\text{AA}}^{\text{f}}$ and $f_{\text{AB}}^{\text{recool}} = \phi_{\text{f}}^{\text{A}} \Phi_{\text{AB}}^{\text{f}}$. While the fluorescence quantum yield, $\phi_{\text{f}}^{\text{A}}$, is a constant, the product quantum yield, $\Phi_{\text{AX}}^{\text{f}}$, from the levels formed by fluorescence are heavily weighted toward the reactant because a significant fraction of the ground state levels reached by fluorescence are below the lowest barrier to isomerization. As Figure 4 shows, this fraction is $(1-0.40) = 0.60$ for *tt*-*m*DVB, 0.51 for *ct*-*m*DVB, and 0.63 for *cc*-*m*DVB. If the above-barrier population is equally distributed between the three conformers, then we predict that $\Phi_{\text{tt} \rightarrow \text{tt}}^{\text{f}} \approx 0.73$, while $\Phi_{\text{tt} \rightarrow \text{cc}}^{\text{f}} = \Phi_{\text{tt} \rightarrow \text{ct}}^{\text{f}} \approx 0.13$. Similar arguments hold for the other conformers. Therefore, while the product channel intensities are not significantly affected by fluorescence, the gain signal in the reactant channels could be reduced. If we set the term in brackets in eq 8a to zero (i.e., $\Phi_{\text{AA}}(E_k) - \phi_{\text{f}}^{\text{A}} \Phi_{\text{AA}}^{\text{f}} = 0$), we deduce a fluorescence quantum yield in *tt*-*m*DVB of $\phi_{\text{f}}^{\text{A}} \sim 0.4$, if indeed fluorescence is the only pathway for return of molecules back to the zero-point level.

TABLE 1: Observed Thresholds to Isomerization and Relative Energies of the Minima in *m*DVB

reactant \rightarrow product	observed bounds to isomerization (cm ⁻¹)	calculated isomerization barriers (cm ⁻¹) ^a
<i>tt</i> \rightarrow <i>ct</i>	1130–1175	1274
<i>tt</i> \rightarrow <i>cc</i>	1130–1175	
<i>cc</i> \rightarrow <i>tt</i>	1080–1232	
<i>cc</i> \rightarrow <i>ct</i>	1080–1232	1208
<i>ct</i> \rightarrow <i>tt</i>	997–1243	1256
<i>ct</i> \rightarrow <i>cc</i>	997–1243	1264
relative energies of minima (cm ⁻¹)		
<i>tt</i>	0	
<i>ct</i>	–113 to +178	
<i>cc</i>	–102 to +95	

^a Difference in energy between the indicated reactant and the transition state separating the reactant and product, corrected for zero-point energy effects.

TABLE 2: Torsional Fitting Parameters

parameters	fit 1a ^a	fit 2a ^b	fit 1b ^c	fit 2b ^d
V_2	671 \pm 30	695 \pm 70	876 \pm 70	769 \pm 54
V_3	–9 \pm 6	16 \pm 10	–1 \pm 5	11 \pm 10
V_4	–239 \pm 11	–207 \pm 30	–321 \pm 10	–317 \pm 9
V_{22}^c	–120 \pm 20	–48 \pm 35	–127 \pm 36	–185 \pm 30
V_{12}^c	–3 \pm 1	15 \pm 7	5 \pm 4	6 \pm 6
V_{22}^s	–19 \pm 2	43 \pm 6	–14 \pm 8	45 \pm 4
V_{12}^s	11 \pm 2	–50 \pm 5	15 \pm 8	–52 \pm 4
DFT symmetry	no	yes	no	yes
sequential barriers (cm ⁻¹)	904–920	754–828	1114–1146	1127–1152
concerted barriers (cm ⁻¹)	1337–1340	1376–1405	1741–1763	1535–1537

^a Unconstrained fit of the observed torsional levels without rotation of the wave functions. While the best-fit values shown in the fits assume independent errors, the values of V_2 and V_4 are highly correlated, leading to a range of fits using the torsional levels alone that have barrier heights that differ substantially from one another. See the preceding paper (ref 1) for details. ^b Unconstrained fit of the observed torsional levels with rotation of the wave functions. See preceding paper (ref 1) for details. ^c Constrained fit of the observed torsional levels without rotation of the wave functions. See text for details. ^d Constrained fit of the observed torsional levels with rotation of the wave functions. See text for details.

IV. Discussion and Conclusions

1. The Isomerization Pathway. Several aspects of our results support the deduction that the lowest energy pathway to isomerization is sequential rather than concerted. The sequential pathway traverses over two lower-energy barriers in which one vinyl “appendage” at a time swings out-of-plane through a perpendicular configuration (with the other remaining in-plane), while a concerted pathway would involve both vinyl groups moving together to perpendicular configurations either on the same or on opposite sides of the phenyl ring (rotatory or counter-rotatory with respect to one another). In the sequential pathway, two low-energy “1D” barriers are traversed in moving between the *tt* and *cc* wells, while the concerted pathway overcomes a second-order saddle point (at $\theta_1 = \theta_2 = \pm\pi/2$). First, a comparison of our measured thresholds with the calculated barriers to isomerization (also included in Table 1) shows a good correspondence with calculation in the barrier heights if sequential pathways are taken. Second, the fact that the same bounds on the thresholds are shared by both *tt* \rightarrow *ct* and *tt* \rightarrow *cc* isomerizations (1130–1175 cm⁻¹) strongly suggests that the

TABLE 3: Observed and Fit Torsional Levels and Isomerization Barriers (Thresholds) in *m*DVB

description	transition	fit 1b (cm ⁻¹)	fit 2b (cm ⁻¹)	obsd data (cm ⁻¹)
<i>cc</i> - ν_{26}	0–1	28	27	[27] ^a
	0–2	55	55	56
	0–3	94	91	[88] ^c
	0–4	135	129	130
	0–5	178	170	[170] ^c
	0–6	223	213	214
<i>cc</i> - ν_{36}	0–1	32	37	[35] ^a
	0–2	76	81	81
	0–3	131	136	[137] ^c
	0–4	190	195	186
<i>tt</i> - ν_{low}	0–1	24	12	[27] ^b
	0–2	52	52	57
	0–3	88	81	[92] ^c
	0–4	127	124	126
	0–5	169	170	[163] ^c
<i>tt</i> - ν_{high}	0–6	214	218	202
	0–1	41	45	[39] ^b
	0–2	88	97	90
	0–3	141	145	[139] ^c
	0–4	199	198	197
	0–5	257	257	257
<i>ct</i> - ν_{54}	0–1	26	23	[31] ^b
	0–2	54	56	70
<i>ct</i> - ν_{53}	0–1	36	39	[37] ^b
	0–2	81	84	86
Sequential Barriers				
<i>tt</i> \rightarrow <i>cc, ct</i>		1146	1152	1130–1175
<i>cc</i> \rightarrow <i>ct, tt</i>		1114	1127	1080–1232
<i>ct</i> \rightarrow <i>tt</i>		1134	1151	997–1232
<i>ct</i> \rightarrow <i>cc</i>		1126	1128	997–1175
av error in torsions		5%	8%	
av error in barriers		2%	2%	

^a Determined by inference from the 1–1 sequence band. These levels were given an error twice as large as those directly observed in the dispersed emission scans because their absolute value was estimated using the constraint imposed by the high-resolution data of Nguyen and co-workers,²² which determined that both ground and excited state geometries were planar. ^b No sequence band data were measurable in the *tt* and *ct* isomers. Estimated values for $\nu = 1$ made using the same assumptions as in footnote a. ^c Estimated values from combination bands with the bend of the same symmetry and the value for the $\nu = 1$ level. The observed error is twice that of other known levels to account for uncertainties in the estimation.

pathway taken by *tt* \rightarrow *cc* isomerization passes over the same rate-limiting barrier as does the *tt* \rightarrow *ct* isomerization. This is the expected consequence of a circumstance in which energy is the dominant factor determining the isomerization pathway. Finally, the roughly equal isomerization product quantum yields deduced from the ratio of SEP–PT intensities (eq 11) indicate that in all cases, $\Phi_{AB}(E_k) \sim F_B$, that is, that the conformational population reaches a near-equilibrium population distribution much like that reached by the conformer population under expansion cooling in the absence of SEP excitation. This would occur if the rate of isomerization is faster than the cooling rate, so that all three conformer wells are sampled by the population on a time scale fast compared to vibrational cooling.

2. Energy Thresholds, Energy Barriers, and Isomerization Product Quantum Yields. Our discussion to this point has made the implicit assumption that the lower and upper bounds to the measured energy thresholds observed in the SEP–PT scans are equivalent to lower and upper bounds on the energy barriers to isomerization. However, the step function in SEP–PT transition intensities in the reactant and product channels provides upper and lower bounds on the barriers to isomerization only if tunneling effects and/or kinetic shifts are negligible.³ Given the substantial mass of the vinyl group, it is unlikely

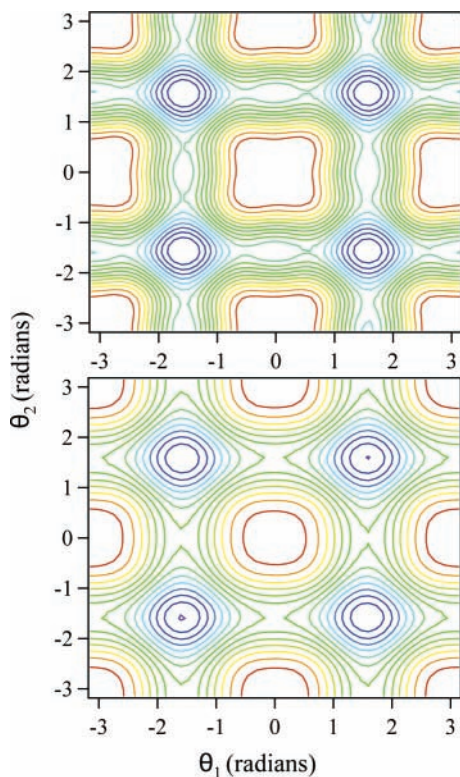


Figure 5. Two-dimensional torsional potential surface of *m*DVB: (top) from fit 1b and (bottom) from DFT/B3LYP//6-31+G* relaxed potential energy scans.

that tunneling will have a measurable effect on these thresholds; however, one cannot immediately dismiss the possibility of a kinetic shift. Since isomerization necessarily occurs in competition with collisional cooling, if the isomerization rate near threshold is much slower than the collisional cooling rate, then the apparent threshold will be shifted to higher energies where the isomerization rate competes successfully with cooling. In past SEP-PT studies,^{4,6} a kinetic shift was apparent by the decreased intensities of the product SEP-PT transitions (relative to the SEP intensities) right near the threshold. In *m*DVB, the most direct evidence for such a competition occurs in the threshold region of the *tt* SEP-PTS scans (Figure 2), where the appearance of the products at 1175 cm⁻¹ (15⁰129¹₁) is accompanied by a decreased intensity in the reactant channel, which undergoes further reduction at 1240 cm⁻¹ to its high-energy limiting value near zero. This argues for a small effect due to this competition, whereby the level at 1175 cm⁻¹ funnels more of its population into the reactant well due to collisional cooling competing with isomerization.

The estimated collision rate with helium at $x/D = 2$ with 7 bar backing pressure behind the nozzle orifice at 298 K nozzle temperature (local expansion temperature at $x/D = 2$ is ~ 36 K) is $\sim 1.6 \times 10^9$ s⁻¹.¹⁵ If we take *tt*-*m*DVB as an example and set the isomerization barrier at 1150 cm⁻¹ (halfway between the lower and upper bounds), then RRKM theory^{16,17} estimates an isomerization rate at a threshold of 3.7×10^8 s⁻¹ if the full density of reactant states participate in reaction. However, since the SEP-PT experiment initially prepares totally symmetric levels, one could argue for a lower density of states by about a factor of 4 and a subsequent threshold isomerization rate of 1.5×10^9 s⁻¹. We do not have a firm knowledge of the average energy lost by *m*DVB per collision with helium, but experience with other large, flexible molecules suggests a fractional energy loss of about 0.3%, equivalent to 3–4 cm⁻¹ per collision at the threshold.^{18,19} A similar fractional energy lost per collision was

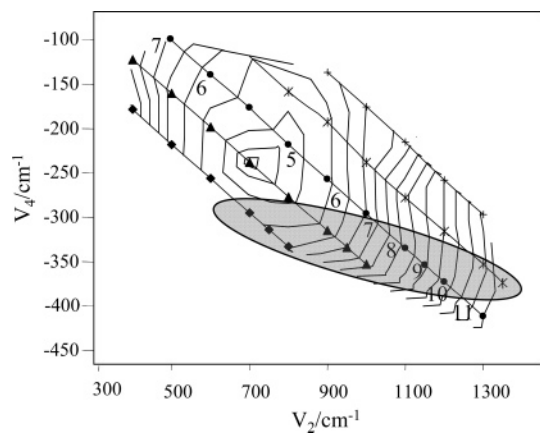


Figure 6. Plot of acceptable sets (average error in torsions $\leq 10\%$) of (V_2, V_4) values from the torsional level fitting of ref 1 for (◆) $V_{22}^c = -200$ cm⁻¹, (▲) $V_{22}^c = -100$ cm⁻¹, (●) $V_{22}^c = 0$ cm⁻¹, (*) $V_{22}^c = 100$ cm⁻¹, and (+) $V_{22}^c = 200$ cm⁻¹. The shaded oval circumscribes the range of values that are consistent with the measured 1D barriers in the range of 1100–1200 cm⁻¹.

determined by Luther and co-workers for highly excited toluene in collisions with helium.^{20,21} These estimates are consistent with the observed intensity effects, in which levels within 20–50 cm⁻¹ of the true threshold are affected but higher levels are not.

Table 1 lists the measured lower and upper bounds on the thresholds, which we now associate with bounds on the barriers to isomerization. Since all six reactant \rightarrow product conformer pairs were measured, combining the threshold measurements for $A \rightarrow B$ and $B \rightarrow A$ leads to the relative energies for the *cc* and *ct* minima listed in Table 1. Not surprisingly, all three conformational minima are within 100 cm⁻¹ of one another in energy.

3. The Two-Dimensional Torsional Surface. In the previous paper,¹ the observed torsional levels were fit to a potential of the form

$$V(\theta_1, \theta_2) = \sum_{n=2-4} \frac{1}{2} V_n (2 - \cos(n\theta_1) - \cos(n\theta_2)) + V_{\text{cross}}$$

where

$$V_{\text{cross}} = V_{12}^c (\cos \theta_1 \cos 2\theta_2 + \cos 2\theta_1 \cos \theta_2) + V_{12}^s (\sin \theta_1 \sin 2\theta_2 + \sin 2\theta_1 \sin \theta_2) + V_{22}^c (\cos 2\theta_1 \cos 2\theta_2) + V_{22}^s (\sin 2\theta_1 \sin 2\theta_2)$$

A major motivation of the present work was to provide an alternative, direct set of measurements of the barriers to isomerization using population transfer methods. With these measurements in hand (Table 1), we return to the torsional potential fitting again to incorporate the new experimental data in the fits.

Using the observed isomerization thresholds from the current study (Table 1) to constrain the range of barrier heights that can be used to fit the torsional level data, we attempted two final fits in the same manner as described in the preceding paper.¹ The values of the fit parameters are given in Table 2 (fit 1b and fit 2b), where they are compared with the fits in which the barrier heights were allowed to move at will (fits 1a and 2a).¹ The resulting torsional level energies and barrier heights are given in Table 3. Fit 1b does not account for the DFT predicted relative frequencies of the lowest torsional levels (see the preceding paper), whereas fit 2b does.

Fits 1a and 2a predict barriers for sequential isomerization (i.e., at $(\theta_1 = 0, \theta_2 = \pm\pi/2)$ and $(\pm\pi/2, 0)$) in the range of 904–920 and 754–828 cm^{-1} , respectively. These are much lower than the measured thresholds in the current study. Furthermore, a strong correlation between V_2 and V_4 was uncovered, in which a range of values of these parameters led to nearly as good a fit as long as $V_4/V_2 = -0.26$ for $-200 \leq V_{22}^c \leq +200 \text{ cm}^{-1}$. This led to a wide range of 1D barrier heights consistent with the torsional level spectroscopic data stretching from 500 to 1400 cm^{-1} .

The best overall fit to all experimental data, including the barrier height measurements of the present work, is fit 1b. In this fit, the average error in the torsional levels and isomerization thresholds are 5% and 2%, respectively. For comparison to the DFT calculated surface, both fit 1b and the DFT computed relaxed potential energy surfaces are shown in Figure 5. Finally, in Figure 6 we also reproduce the figure containing the set of correlated acceptable potential parameter values from the preceding paper, with the range of fits consistent with the experimental 1D barrier heights ($\sim 1100\text{--}1200 \text{ cm}^{-1}$) overlaid on it (the shaded oval) for comparison. Clearly, the barrier height data greatly reduce the uncertainty in the potential fit, with the torsional level and barrier height measurements placing complementary constraints on the surface properties. Such a combination of spectroscopy and direct barrier measurements forms a powerful means by which one can extend the accuracy of experimental determinations of key elements of potential energy surfaces of greater complexity than has been previously possible. Of course, even this combination of methods has its limitations, since hole-filling methods determine the lowest energy thresholds and thus are not sensitive to other saddle points, such as the concerted 2D barrier in *m*DVB.

Acknowledgment. The authors gratefully acknowledge the support of the Department of Energy Basic Energy Sciences, Division of Chemical Sciences under Grant No. DE-FG02-96ER14656.

References and Notes

- (1) Selby, T. M.; Meerts, W. L.; Zwier, T. S. *J. Phys. Chem. A* **2006**, *111*, 3697–3709.
- (2) Dian, B. C.; Clarkson, J. R.; Zwier, T. S. *Science* **2004**, *303*, 1169–73.
- (3) Clarkson, J. R.; Dian, B. C.; Moriggi, L.; DeFusco, A.; McCarthy, V.; Jordan, K. D.; Zwier, T. S. *J. Chem. Phys.* **2005**, *122*, 214311.
- (4) Clarkson, J. R.; Baquero, E.; Zwier, T. S. *J. Chem. Phys.* **2005**, *122*, 214312.
- (5) Clarkson, J. R.; Baquero, E.; Shubert, V. A.; Myshakin, E.; Jordan, K. D.; Zwier, T. S. *Science* **2005**, *307*, 1443–6.
- (6) Selby, T. M.; Clarkson, J. R.; Mitchell, D.; Fitzpatrick, J. A. J.; Lee, H. D.; Pratt, D. W.; Zwier, T. S. *J. Phys. Chem. A* **2005**, *109*, 4484.
- (7) Zwier, T. S. *J. Phys. Chem. A* **2006**, *110*, 4133–50.
- (8) Burgi, T.; Droz, T.; Leutwyler, S. *Chem. Phys. Lett.* **1995**, *246*, 291–9.
- (9) Burgi, T.; Droz, T.; Leutwyler, S. *J. Chem. Phys.* **1995**, *103*, 7228.
- (10) Zwier, T. S. *J. Phys. Chem. A* **2001**, *105*, 8827–39.
- (11) Silva, M.; Jongsma, R.; Field, R. W.; Wodtke, A. M. *Annu. Rev. Phys. Chem.* **2001**, *52*, 811–52.
- (12) Dian, B. C.; Longarte, A.; Zwier, T. S. *Science* **2002**, *296*, 2369–73.
- (13) Dian, B. C.; Longarte, A.; Winter, P. R.; Zwier, T. S. *J. Chem. Phys.* **2004**, *120*, 133–47.
- (14) Dian, B. C.; Florio, G. M.; Clarkson, J. R.; Longarte, A.; Zwier, T. S. *J. Chem. Phys.* **2004**, *120*, 9033–46.
- (15) Lubman, D. M.; Rettner, C. T.; Zare, R. N. *J. Phys. Chem.* **1982**, *86*, 1129–35.
- (16) Marcus, R. A. *J. Chem. Phys.* **1952**, *20*, 359.
- (17) Baer, T.; Hase, W. L. *Unimolecular Reaction Dynamics: Theory and Experiments*; Oxford University Press: Oxford, U.K., 1996.
- (18) Dian, B. C.; Florio, G. M.; Clarkson, J. R.; Longarte, A. *J. Chem. Phys.* **2004**, *120*, 9033.
- (19) Dian, B. C.; Longarte, A.; Winter, P. R.; Zwier, T. S. *J. Chem. Phys.* **2004**, *120*, 133.
- (20) Lenzer, T.; Luther, K.; Reihs, K.; Symonds, A. C. *J. Chem. Phys.* **2000**, *112*, 4090–110.
- (21) Hold, U.; Lenzer, T.; Luther, K.; Reihs, K.; Symonds, A. C. *J. Chem. Phys.* **2000**, *112*, 4076–89.
- (22) Nguyen, T. V.; Ribblett, J. W.; Pratt, D. W. *Chem. Phys.* **2002**, *283*, 279–87.